Angewandte
Eine Zeitschrift der Gesellschaft Deutscher Chemiker
Chemie

Supporting Information

Electrochemical Dynamics of a Single Platinum Nanoparticle Collision Event for the Hydrogen Evolution Reaction

Zhi-peng Xiang[+], Hai-qiang Deng[+], Pekka Peljo, Zhi-yong Fu, Su-li Wang, Daniel Mandler, Gong-quan Sun, and Zhen-xing Liang**

anie_201712454_sm_miscellaneous_information.pdf

Table of Contents	**Page**

EXPERMENTAL

***Reagents and Materials*.** Sodium citrate-capped Pt nanoparticles with an average diameter of 70 nm from nanoComposix (San Diego, United States) were characterized by scanning electron microscopy (SEM) (see Figure S1 and Table S1). Perchloric acid (Kermel, 72%, AR) and sodium citrate (Sinopharm Chemical Reagent Co., Ltd, AR) were used as received without further purification. Helium (99.999%) was provided by Guangzhou Shengying Gas Co., Ltd, and hydrogen (99.999%) was produced by a QL-200 Hydrogen Generator, Shandong Saikesesi Hydrogen Energy Co., Ltd. All aqueous solutions were prepared from deionized water (≥ 18.2 MΩ cm).

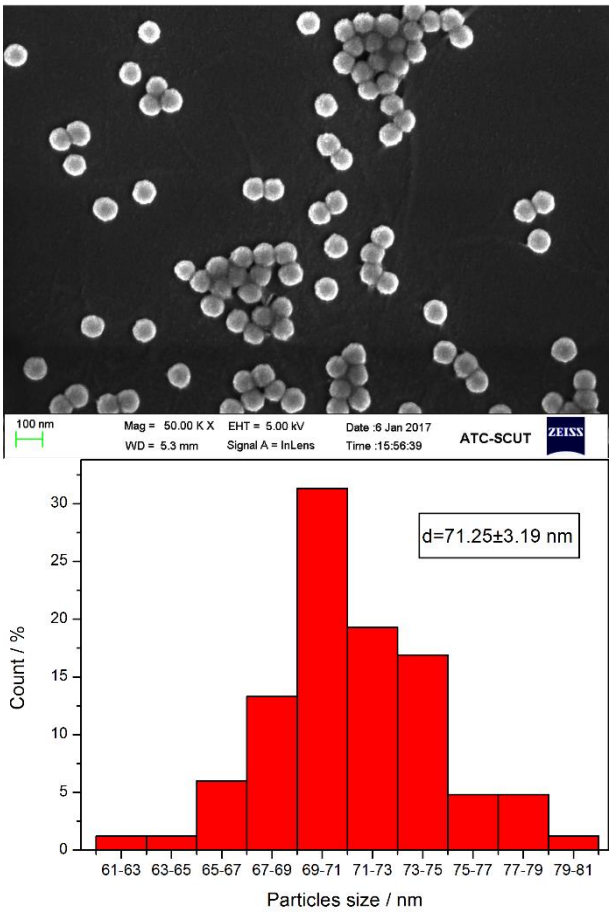

Figure S1. SEM image of commercial 70 nm Pt NPs (upper panel), and size distribution of 80 Pt NPs from SEM (lower panel).

Table S1. Information of commercial platinum colloidal dispersion.

Diameter (vendor)	Mass concentration (Pt)	Particle concentration	Hydrodynamic diameter (DLS)	Measured pH of solution
72.2 ± 4.2 nm	0.052 mg ml^{-1}	1.2E+10 particles ml^{-1}	85 nm	7.8

***Instrumentation*.** All voltammetric measurements were performed using a CHI model 660E potentiostat with a one-compartment three-electrode glass cell housed in a Faraday cage. Home-made Au and Pt ultramicroelectrodes[1] (both in 25 μm diameter) act as the working electrodes, with Ag/AgCl (saturated KCl) as the reference electrode, and an Au wire as the counter electrode. Before each voltammetric experiment or chronoamperometry, the working electrode was polished with a polishing film (0.02 μm silicon carbide) to a mirror surface. Note that all the electrode potentials were reported versus standard hydrogen electrode (SHE) unless otherwise mentioned, by the relation of $E_{Ag/AgCl} = E_{SHE} + 0.197$ (V).[2] Referring to overpotential, reversible hydrogen electrode (RHE) is used as the reference electrode, by the relation of $E_{RHE} = E_{SHE} - 0.059pH$ (V).

All electrolyte solutions were thoroughly saturated with either helium or hydrogen or hydrogen/helium mixture in voltammetric measurements. Specifically, 10 ml of 1.0 mM perchloric acid electrolyte was firstly deoxygenated by purging with helium for 30 min followed by bubbling helium, hydrogen or hydrogen/helium mixture for 30 min to saturate the solution. During the gas saturation, 0.30 ml of Pt NP colloid (1.2×10^{10} particles ml^{-1}, see Table S1) was added, thus achieving a Pt NP solution of 0.58 pM. Finally, we would like to note that hydrogen volumetric flow rate is controlled $\geq$ 100 ml min^{-1} such that the solution is fully saturated (see Figure S2 & Table S2, and corresponding discussion in details, *vide infra*).

The colloidal stability was investigated by an *ex-situ* method, *viz.* dynamic light scattering (DLS). The test was performed by a Brookhaven Zeta instrument with the above Pt NP solutions at the time of 0, 120, 300, 600, 1200, and 1800 s. Each test takes two cycles, and one cycle lasts 30 s. The DLS cell was sealed under helium, hydrogen or ambient atmosphere during the whole test period.

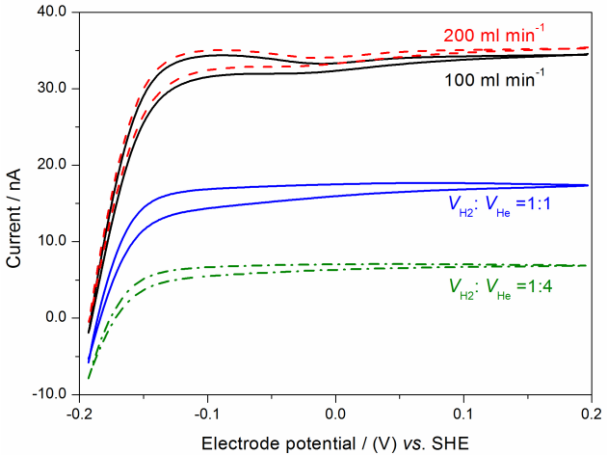

Figure S2. Cyclic voltammograms (CVs) of HOR on Pt UME (25 μm in diameter) in 1 mM $HClO_4$ solution with different volumetric flow rates and partial pressures of hydrogen (detailed in Table S2) at the scan rate of 50 mV s^{-1}. Potential scale: SHE.

Table S2. The concentration of hydrogen in test solutions with different volumetric flow rates and partial pressures of hydrogen.

	V_{total} = 100 ml min^{-1}			V_{H_2} = 200 ml min^{-1}
	V_{H_2} :V_{He}=1:0	V_{H_2} :V_{He}=1:1	V_{H_2} :V_{He}=1:4	
i / nA	34.5	17.4	6.90	35.5
c_{H_2} / mM	0.794	0.398	0.158	0.820

We studied the effect of the volumetric flow rate of hydrogen on H_2 supersaturation by CVs recorded at a Pt UME (25 μm in diameter), as seen in Figure S2. Hydrogen concentration in the bulk solution is then calculated from the diffusion-limited steady-state anodic current by Equation S1.

$$i_{\lim} = 4nFDcr \quad \text{(S1)}$$

where $i_{\lim}$ is the diffusion-controlled steady-state anodic current of UME, D is the diffusion coefficient of reactant (here H_2, 4.5 × 10^{-5} cm^2 s^{-1}, cf. *AIChE J. 1967, 13, 702*), c is the concentration of reactant, F is the Faraday constant, n is the number of charge transfer (= 2), and r represents UME's geometric radius.

The anodic part of the CV is shown to clarify the calculations. The results show that the concentration of hydrogen in 1.0 mM $HClO_4$ solution is 0.79 mM (see Table S2) at the volumetric flow rate of 100 ml min^{-1} (black trace in Figure S2), which is consistent with the reported value (0.78 mM) in literature[3] and the calculated value by Henry's law (0.79 mM, see Equation S11). H_2 concentration increases slightly to 0.82 mM (see Table S2) at the volumetric flow rate of 200 ml min^{-1} (dashed red trace in Figure S2), implying the supersaturation of H_2.

In terms of single nanoparticle collision electrochemistry, much attention has been drawn to employ hydrazine oxidation and/or proton reduction as the redox indicator reaction.[4] As reported by Bard and co-workers,[5] NP aggregation occurs when proton concentration exceeds 10.0 mM for 4 nm Pt NPs; however, the acid-induced NP aggregation has not been well understood yet. In previous works, concentrated electrolyte solutions, such as 10 mM $HClO_4$,[5] 50 mM sodium

dihydrogen citrate[5-6] and 50 mM phosphate buffer (pH ~ 4.0),[7] have been widely used as the proton source, in which Pt NPs however tend to aggregate.[6] As such, stable and discrete ECA signals of non-aggregated single NP collisions towards the HER have not been observed in the investigated experimental timescale. Herein, we firstly addressed the dynamic stability of the Pt NPs by monitoring the ECA signals of HER at the same overpotential of 0.10 V *vs*. RHE (Figure S3A and Table S3) when Pt NPs (diameter: 70 nm, see Figure S1 and Table S1) collide with an inert gold UME in $HClO_4$ solutions of variable concentrations (*i.e.* proton concentration).

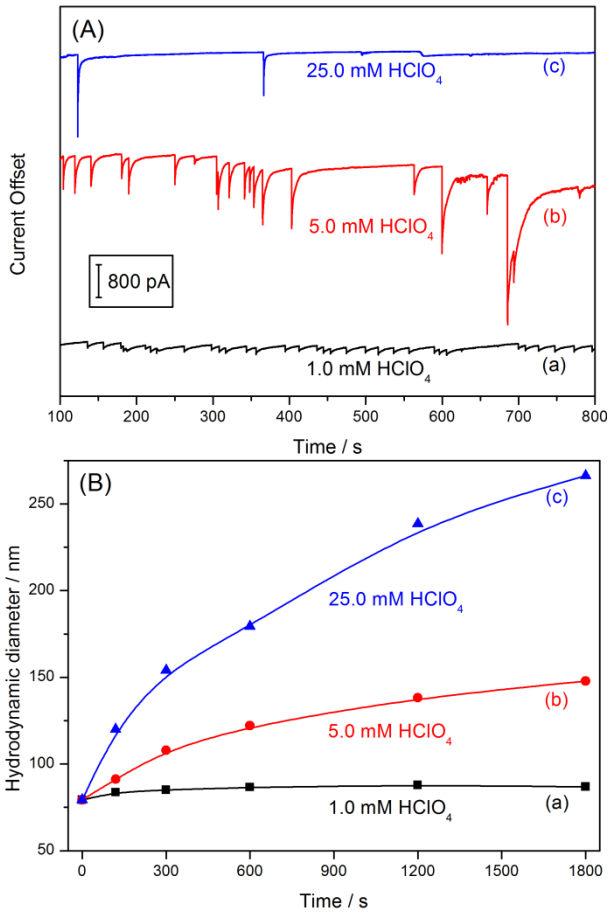

Figure S3. (A) Amperometric *i*–*t* curves of 0.58 pM 70 nm Pt NP collisions on a 25 µm Au UME in He-saturated solutions (a) 1.0 mM $HClO_4$, (b) 5.0 mM $HClO_4$, (c) 25.0 mM $HClO_4$ at the same overpotential of 0.10 V (see Table S3). (B) Dynamic light scattering results of the Pt NP hydrodynamic diameters *vs*. time in air.

As shown in the *i-t* curves in Figure S3A, uniform current transients with respect to peak height and duration are observed in 1.0 mM $HClO_4$ solution (black trace in Figure S3A), indicating that individual nanoparticles rather than aggregates collide with the electrode surface. In comparison, inhomogeneous current magnitudes, irregular time intervals and lower impact frequencies of the ECA signals are observed in 5.0 mM $HClO_4$ solution (red trace in Figure S3A), indicating that NPs are unstable and aggregate in the colloidal dispersion. Using an even higher $HClO_4$ concentration of 25 mM (blue trace in Figure S3A), a much lower impact frequency indicates a more serious aggregation process, which yields larger aggregates and thus decreases both the molar concentration and diffusion coefficient. The measured impact frequencies are *ca*. 0.05, 0.03, 0.004 Hz (s^{-1}) (see Figure S4) for 0.58 pM of 70 nm Pt NPs (hydrodynamic diameter = 85 nm, see Table S1) colliding with a 25 µm diameter Au UME in 1.0, 5.0, and 25.0 mM $HClO_4$ solutions, respectively. Bard *et al.*[5] reported a collision frequency of *ca*. 0.04 Hz when 25 pM of 4 nm Pt NPs collide with a 8 µm diameter carbon UME in 50 mM sodium dihydrogen citrate solution. However, the theoretical collision frequency based on their experimental conditions is calculated to be 29.62 Hz (Equation S7, *vide infra*). Note that they further used 10 mM $HClO_4$ + 20 mM

$NaClO_4$ as the working solution for the NP collisions, in which the collision frequency is even lower than the above-mentioned 0.04 Hz.[5] This significant deviation reveals the key role of the proton concentration in determining the colloidal stability. The theoretical collision frequency of the NPs dictated solely by NP diffusion to an infinite electrode surface, $f_{p,s}$, can be estimated by Equations S2-3.[8]

Table S3. Applied electrode potentials in Figure S3A *vs*. Ag/AgCl, SHE and RHE in solutions with different proton concentrations.

proton concentration / mM	1.0	5.0	25.0
***E* / V (*vs*. Ag/AgCl)**	−0.49	−0.44	−0.40
***E* / V (*vs*. SHE)**	−0.293	−0.243	−0.203
E* / V (*vs*. RHE)	−0.10	−0.10	−0.10

(*standard pressure is used in the calculation.)

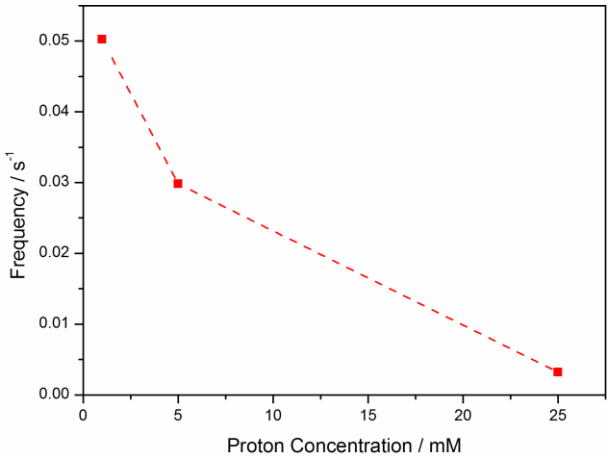

Figure S4. The collision frequency *vs.* proton concentration.

$$f_{p,s} = 4D_p c_p r_{UME} N_A \quad \text{(S2)}$$

$$D_p = \frac{k_B T}{6\pi\eta r_p} \quad \text{(S3)}$$

where D_p is the diffusion coefficient of the Pt NPs, c_p is the molar concentration of the NPs, r_{UME} is the radius of the Au UME, N_A is Avogadro's number, k_B is the Boltzmann constant, T is the thermodynamic temperature, η is the dynamic viscosity of water at 298.15 K (0.89×10^{-3} kg m^{-1} s^{-1}),[9] and r_p is the radius of the NPs.

The calculated collision frequency is 0.09 Hz (see Equation S5) for 0.58 pM of 70 nm (calculated using the hydrodynamic diameter, 85 nm) Pt NPs colliding with a 25 µm UME.

In our case, r_p = 42.5 nm, c_p = 0.58 pM, and r_{UME} = 12.5 µm; hence, the diffusion coefficient D_p is calculated as follows,

$$D_P = \frac{1.38*10^{-23}\,\mathrm{J/K}*298.15\ \mathrm{K}}{6*3.14*0.89*10^{-3}\,\mathrm{kg/ms}*42.5*10^{-9}\ \mathrm{m}} = 5.77*10^{-12}\ \mathrm{m^2/s} \quad \text{(S4)}$$

The collision frequency $f_{p,s}$ is estimated,

$$f_{p,s} = 4*5.77*10^{-12}\ \mathrm{m^2/s}*0.58*10^{-9}\,\mathrm{mol/m^3}*12.5*10^{-6}\ \mathrm{m}*6.02*10^{23}\ \mathrm{mol^{-1}} = 0.09\ \mathrm{s^{-1}} \quad \text{(S5)}$$

In Ref. (Bard *et al.*),[5] r_p = 2 nm, c_p = 25 pM , r_{UME} = 4 µm,

$$D_P = \frac{1.38*10^{-23}\,\mathrm{J/K}*298.15\ \mathrm{K}}{6*3.14*0.89*10^{-3}\,\mathrm{kg/ms}*2*10^{-9}\ \mathrm{m}} = 1.23*10^{-10}\,\mathrm{m^2/s} \quad \text{(S6)}$$

And the collision frequency $f_{p,s}$,

$$f_{p,s} = 4*1.23*10^{-10}\ \mathrm{m^2/s}*25*10^{-9}\,\mathrm{mol/m^3}*4*10^{-6}\ \mathrm{m}*6.02*10^{23}\ \mathrm{mol^{-1}} = 29.62\ \mathrm{s^{-1}} \quad \text{(S7)}$$

The experimental collision frequency of 0.05 Hz (for 1.0 mM $HClO_4$) is a bit lower than the theoretical value of 0.09 Hz, in which this discrepancy might originate from the experimental errors, ineffective collision events,[10] Fermin-level equilibrium of NP in close contact with the electrode,[11] and the near-wall hindered diffusion.[12] The near-wall hindered diffusion, which has been explicitly investigated by Compton and co-workers,[12] describes the distance-dependent

reduction of the NP's diffusion coefficient in the impact region of a UME with respect to the bulk diffusion coefficient. Nevertheless, the deviation of the experimental collision frequency from the theoretical one is much less significant than that reported by Bard *et al*..[5] This remarkable deviation reported in the literature[5] strongly indicates that the Pt NPs experience serious aggregation/agglomeration during the collection of *i*−*t* curves.

The stability of colloids can be understood as follows. Derjguin-Landau-Verwey-Overbeek (DLVO) theory suggests that the electrostatic repulsive force between NPs having alike charges is larger than the van der Waals attractive force, leading to a lower collision probability between NPs and keeping them physically apart from each other.[13] The Pt NPs used in this work are capped with negatively charged citrate, which contributes to the stability of the colloids. Citric acid has three pK_a values: 3.13, 4.76 and 6.40. As such, in 1.0 mM $HClO_4$ (experimentally measured pH = 3.20, Table S4), the Pt NPs carry sufficiently negative charge to give rise to electrostatic repulsive force so as to stabilize the colloids. In comparison, when the $HClO_4$ concentration is increased to 5.0 (pH=2.39, Table S4) or 25.0 (pH=1.67, Table S4) mM, the capping agent is protonated and the surface gets mostly neutralized, which seriously destabilizes the colloidal dispersion.

Table S4. pH of the experimental solutions.

proton concentration / mM	1.0	5.0	25.0
pH	3.06	2.35	1.66
pH*	3.20	2.39	1.67

(*pH of the solution: $HClO_4$ solution (10.00 ml) + Pt NP colloid (0.30 ml))

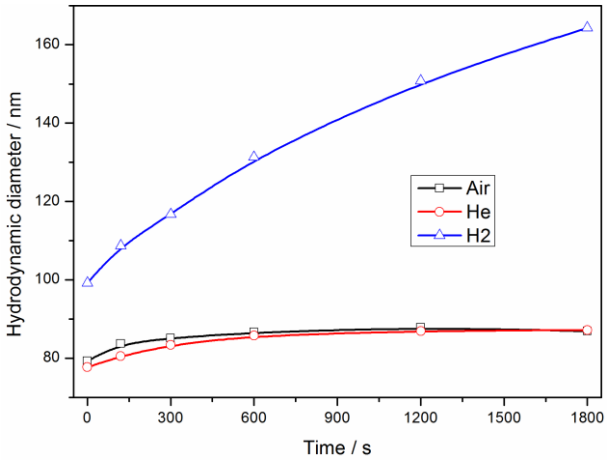

Figure S5. Dynamic light scattering results of the hydrodynamic diameters of the Pt NPs *vs*. time in air-saturated (black trace), helium-saturated (red trace) and hydrogen-saturated (blue trace) 1.0 mM $HClO_4$ solution.

To corroborate the ECA collision results, DLS was adopted to track the dynamic status of the NPs as a function of time at the three $HClO_4$ concentrations. Figure S3B shows the relation between hydrodynamic diameter and time under ambient atmosphere. In 1.0 mM $HClO_4$ electrolyte, the Pt nanoparticle size does not change observably within the investigated timescale, which implies that the dispersion remains stable at least for 30 min in air (black trace in Figure S3B), and the same behavior is observed in He atmosphere (see Figure S5). When the $HClO_4$ concentration increases to 5.0 mM (red trace in Figure S3B), the Pt NPs become unstable, start to aggregate and continuously grow to ~130 nm within 30 min. This aggregation is remarkably accelerated at an even higher $HClO_4$ concentration of 25.0 mM (blue trace in Figure S3B). In other words, the higher the proton concentration is, the faster the aggregation occurs. The good correlation between ECA collision and DLS results demonstrates the feasibility and validity of our experimental conditions. Specifically, the Pt NPs remain stable in 1.0 mM $HClO_4$ electrolyte in the timeframe of the electrochemical collision experiments, ensuring that the genuine ECA response resulting from a collision of a single NP can be observed. In comparison, the NP aggregation occurs under H_2 atmosphere, even in 1.0 mM $HClO_4$ solution (blue trace in Figure S5).

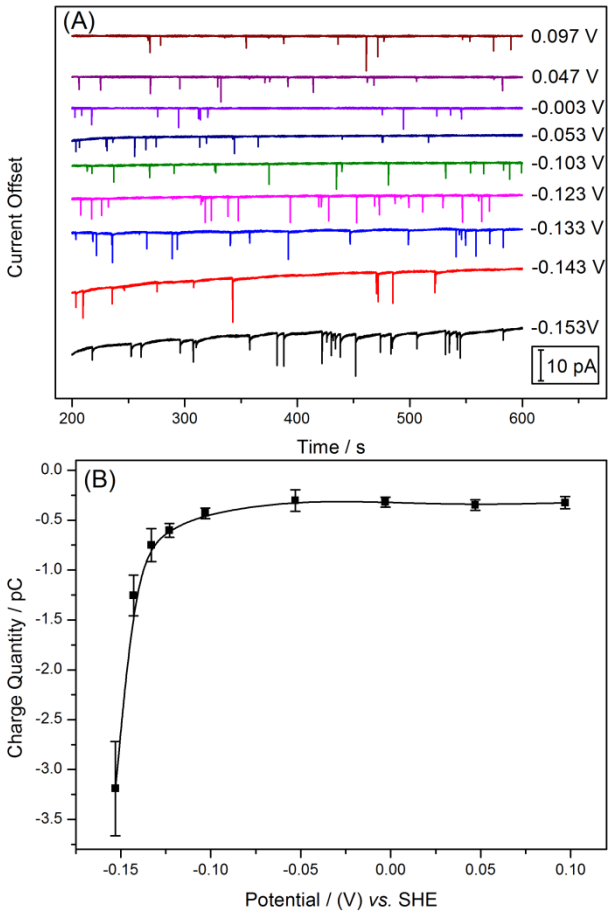

Figure S6. (A) Amperometric *i*–*t* curves of 0.58 pM 70 nm Pt NPs collisions on the 25 µm (diameter) gold UME biased at potentials mainly within the hydrogen-under-potential-deposition region (*vs*. SHE) in He-saturated 1.0 mM $HClO_4$ solution; (B) the corresponding average charge transferred for the spikes from panel A as a function of the applied potential.

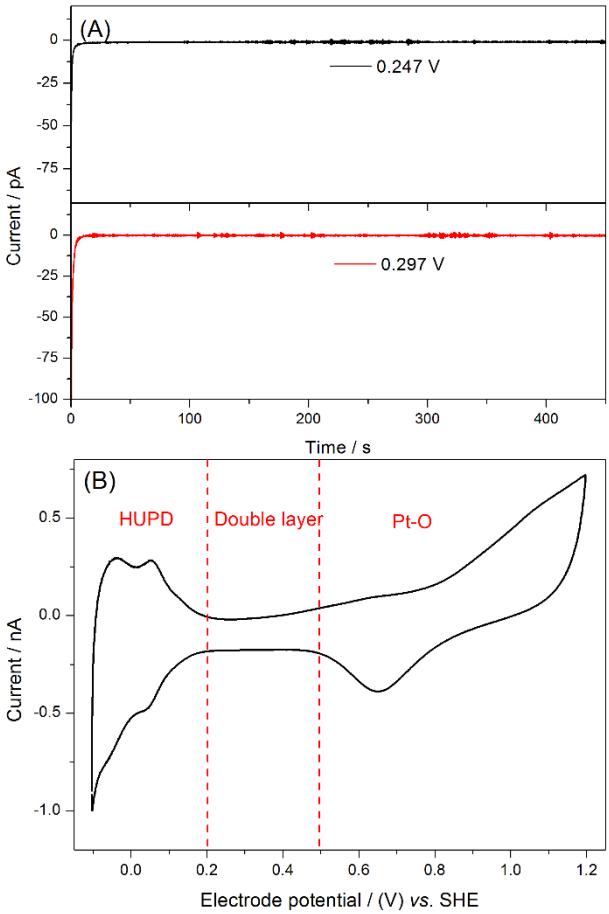

Figure S7. (A) Amperometric *i*−*t* curves of 0.58 pM Pt NP collisions on a 25 μm gold UME held at 0.247 (black curve) and 0.297 V (red curve) in He-saturated 1.0 mM $HClO_4$ test solution; (B) CV of Pt UME (25 μm in diameter) in He-saturated 1.0 mM $HClO_4$ at a scan rate of 50 mV s^{-1}. Potential scale: SHE.

A staircase rather than spike current profile should be seen in Figure S3A as the applied overpotential is located at the H^+ diffusion-limited HER potential region. To clarify this issue, we carried out the Pt NPs electrochemical collision experiments in He-saturated 1.0 mM $HClO_4$ within and around the hydrogen-under-potential-deposition (H_{UPD}) region as shown in Figure S6A. The average charge transferred upon collision is further plotted as a function of potential, as shown in Figure S6B. HER onset potential is determined to be −0.13 V *vs*. SHE from Figure S6. Figure S7 displays the electrochemical collision data at the double-layer region (upper panel) and a CV of 25 μm Pt UME in He-saturated 1.0 mM $HClO_4$ (lower panel), respectively. So far, it clearly proves that the discrete spiky current in Figure S3A is indeed originated from HER instead of H_{UPD}, capacitive current, or reduction of either oxygen or platinum oxide. However, the attenuated current behavior of each collision event in Figure S3A remains unclear. Does the NP collide with the UME and then move back to the bulk solution that accounts for this current decay? Nevertheless, the CVs in Figure S8 indicate that the collided Pt NPs stick onto the Au UME after their landings, rather than dance and leave the electrode after impacting the UME.

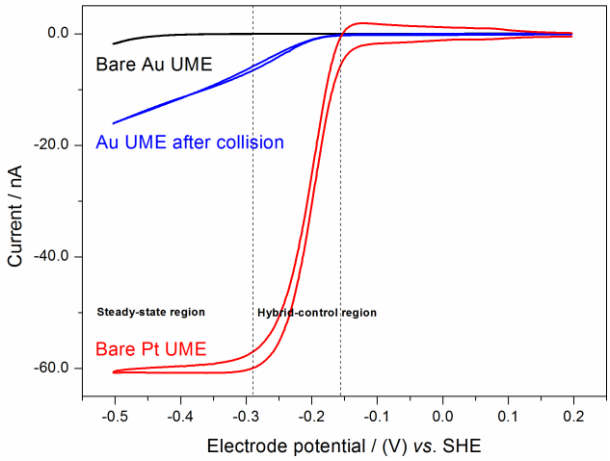

Figure S8. Cyclic voltammograms of different UMEs recorded in 1.0 mM $HClO_4$ solution at a scan rate of 50 mV s^{-1} under helium atmosphere, with Ag/AgCl (saturated KCl) as the reference electrode, and a gold wire as the counter electrode: a bare 25 µm Au UME (black trace), a 25 µm Au UME after the collision electrochemical experiment as being conducted in the black trace in Figure S3A (blue trace), and a bare 25 µm Pt UME (red trace). Notes: potential is corrected in the SHE scale.

The black and red traces in Figure S8 respectively correspond to a bare Au and Pt UMEs in a fresh He-saturated 1.0 mM $HClO_4$ solution. Unsurprisingly, in the potential range between 0.2 and −0.4 V, the bare Au UME has only negligible non-Faradaic capacitive current, while the Pt UME exhibits its characteristic catalytic current towards the HER with a low onset potential at *ca.* −0.16 V *vs.* SHE. The onset potential estimated in Figure S8 is very close to that determined in Figure S6. The blue trace in Figure S8 represents the CV of the Au UME after the collision experiment with 70 nm diameter Pt NPs in 1.0 mM $HClO_4$ solution (*viz.* black trace in Figure S3A). The presence of a remarkable HER current directly suggests that the collided Pt NPs stick onto the Au UME after collision. It is, thus, inferred that the collision HER electrochemistry should yield a staircase current if a sufficient overpotential is applied to reach the mass-transfer control. We further collected more amperometric curves at other potentials to corroborate the above conjecture (Figure 1 in the main text and Figures S9−10).

Nernst equation for hydrogen evolution reaction

The HER can be written as Equation S8,

$$2H^{+}_{(aq)} + 2e^{-} \leftrightarrow H_{2(g)} \quad \text{(S8)}$$

The corresponding Nernst equation is written as Equation S9,

$$E_{H^+/H_2} = E^{\ominus}_{H^+/H_2} + \frac{RT}{nF}\ln\left[\frac{(a_{H^+})^2}{\varphi_{H_2} p_{H_2}/p^{\ominus}}\right] \quad \text{(S9)}$$

where E_{H^+/H_2} is the electrode equilibrium potential (in V), $E^{\ominus}_{H^+/H_2}$ is the standard hydrogen electrode potential that is 0 V by definition, R is the universal gas constant, F is the Faraday constant, n is the number of charge transfer (n = 2), a_{H^+} is the activity of proton (dimensionless), φ_{H_2} is the fugacity coefficient of hydrogen (dimensionless, assumed to be 1), p_{H_2} is the partial pressure of hydrogen (in kPa), $p^{\ominus}$ is the standard pressure (101.325 kPa), and T has been defined before.

The electrode potential for the HER shown in Equation S9 can also be expressed in terms of the concentration of participated redox active species, and hence, the equilibrium potential is given in terms of the formal potential ($E^{\ominus\prime}_{H^+/H_2}$).

$$E_{H^+/H_2} = E^{\ominus\prime}_{H^+/H_2} + \frac{RT}{2F}\ln\left[\frac{\left(c_{H^+}/c^{\ominus}\right)^2}{c_{H_2}/c^{\ominus}}\right] = E^{\ominus\prime}_{H^+/H_2} + \frac{RT}{F}\ln\left[\frac{c_{H^+}}{c_{H_2}^{1/2} c^{\ominus 1/2}}\right] \quad \text{(S10)}$$

where c_{H^+} and $c^{\ominus}$ represent proton concentration (in mol dm^{-3}) and standard concentration (1 mol dm^{-3}), respectively. c_{H_2} is the solubility of H_2 in a dilute solution and obeys the Henry's law, as shown below.

$$c_{H_2} = b_{H_2} \times \rho_{H_2O} = \frac{p_{H_2}}{k_{H_2}} \times \rho_{H_2O} \quad \text{(S11)}$$

where b_{H_2} is the molality of H_2 (in mol kg^{-1}), ρ_{H_2O} is the density of pure water (0.99709 kg dm^{-3}),[14] and k_{H_2} is the Henry's law constant of H_2 (1.28×10^5 kPa kg mol^{-1}) at 298.15 K. The solubility of H_2 under the standard pressure is calculated to be 0.79 mM by using Equation S11. This value is consistent with the experimental results (see Table S2) and the reported value of 0.78 mM.[3]

Comparing Equation S9 and Equations S10-11, we could obtain the expression of the formal potential for the H^+/H_2 redox couple, depicted in Equation S12.

$$E^{\ominus\prime}_{H^+/H_2} = E^{\ominus}_{H^+/H_2} + \frac{RT}{F}\ln\left[\frac{\gamma_{H^+} p^{\ominus 1/2} \rho_{H_2O}^{1/2}}{c^{\ominus 1/2} \varphi_{H_2}^{1/2} k_{H_2}^{1/2}}\right] \quad \text{(S12)}$$

where γ_{H^+} represents activity coefficient of protons and φ_{H_2} and $p^{\ominus}$ have been defined before.

Thermodynamics analysis: drift in equilibrium potential

Regarding the drift in equilibrium potential, thermodynamics − Nernst equation of HER has been analyzed (*vide supra*). Equation S10 shows that the equilibrium potential is determined by the activity/concentration of proton and the partial pressure/concentration of hydrogen together. The proton concentration decreases and the hydrogen concentration increases at the NP/electrolyte interface as the HER proceeds during the chronoamperometric experiments in He-saturated solutions. Therefore, the equilibrium potential of the HER could drift towards more negative potentials rather than be poised over time, albeit the electrode potential applied at the Au UME from the potentiostat is kept apparently constant. This drift may shift the HER from diffusion-limited to kinetics-controlled potential range, especially when biasing the UME at less negative potentials. Figure 1A in the main text shows that the current profile at –0.403 V, –0.343 V, and –0.243 V features a staircase, a spike-staircase hybrid, and a spike, respectively. They correspond to HER diffusion zone, diffusion/kinetics mixture zone, and kinetics zone, respectively. Details on the current profile transition at varying potentials under He can be seen from "a" to "e" panels in Figure S9. We also excluded the scenario of "adsorption of Pt NPs on the underlying UME is potential-dependent" to account for this current feature evolution, as spikes rather than staircases will be seen when the UME is polarized at more negative potentials: the cathodic polarization results in stronger electrostatic repulsion between the negatively-charged NP and the negatively-charged UME, and the consequent NP's detachment from UME.

To further support the above analysis, the amperometric *i*−*t* curves were collected under the same conditions except using H_2-saturated solution, as seen in Figure 1B in the main text. In such case, the bulk hydrogen concentration is kept constant during the experiment, and the only time-dependent variable is the proton activity. It is notable that as the proton transfer is extremely fast in water, the interfacial proton concentration on the nanoscopic electrode (of Pt NP in good electrical contact with the UME) can be well defined at a given potential by the Nernst equation (Equation S10). Therefore, the applied overpotential on the UME (and also on the intimately attached NP) can be poised. In line with this analysis, the current signal is a staircase for each collision event, which is independent of the potentials from −0.203 to −0.403 V, as displayed in Figure 1B in the main text. Regarding the details, one can refer to a zoom-in current transient at −0.293 V in hydrogen-saturated solution in panel "f" in Figure S9. This finding indicates that the diffusion-controlled steady-state current can be readily reached upon the NP collision in H_2-saturated solution. Amperometric curves of the collision events in a He-H_2 mixture with different partial pressures of hydrogen are shown in Figure S10 (see Figure S2, Table S2 for the concentration of hydrogen). It is seen that the current transient remains staircase when the partial pressure of hydrogen is decreased to 0.5 atm and even to 0.2 atm, which is independent of the applied potential. This result confirms that the steady state is much easier to be achieved provided that a given concentration of hydrogen is present in the bulk solution (*vide supra*). And noteworthy, the current magnitude remains unchanged when the partial pressure of hydrogen drops dramatically from 1 to 0.2 atm, which is understandable as the reaction rate is limited by the diffusion of protons and proton concentration remains the same in each experiment. It is, thus, concluded that the interfacial dynamics plays a key role in determining the current transient shape, besides the poisoning and the deactivation effect of the NP surface.

Blocking effect of hydrogen bubble

One may raise the concern that the spiky current profile in He atmosphere originates from the blocking effect of bubble formation of hydrogen on the NP surface. In this work, the blocking effect can be excluded due to the following two reasons: (1) A very low initial concentration of H^+, 1.0 mM $HClO_4$, is used so that the generated hydrogen can be dissolved in solution; (2) If gas bubbles can block the Pt surface, spikes rather than staircases will be seen, which should be more serious in H_2-saturated solution than He-saturated one. Besides, unlike the work of White's group,[15] the CVs of HER at either Au (Figure S12) or Pt (Figures S8, S13) UME are smooth in shape and a constant limiting current of HER is achieved. This result intuitively indicates that no bubbles are generated and block the steady-state diffusion of protons.

COMSOL simulations (more details, *vide infra*) show that under 100% He atmosphere, the equilibrium concentration of hydrogen at the electrochemical interface is always below the saturation limit of 0.79 mM (Table S5). Even at a partial hydrogen pressure of 0.2 atm, the equilibrium concentration of hydrogen still remains lower than the saturation limit in the investigated potential range. In such cases, it is unlikely for the hydrogen bubbles to form on the surface of Pt NPs. In comparison, at a partial hydrogen pressure above 0.5 atm, the equilibrium concentration of hydrogen at a sufficiently negative potential (*e.g.* −0.293 V) exceeds the saturation limit (Table S5). As such, the formation of gas bubbles is excluded from consideration as the bubbles will hinder the diffusion of protons and consequently decrease the current magnitude of NPs collision. Besides, the oxide on the Pt NP surface is unlikely to have a detectable effect on the HER behavior (see Figure S7), as the onset reduction potential of Pt-O to Pt is *ca*. 0.8 V *vs*. SHE.[2] As such, the two factors proposed in this work to explain the shape of the current transition are reasonable.

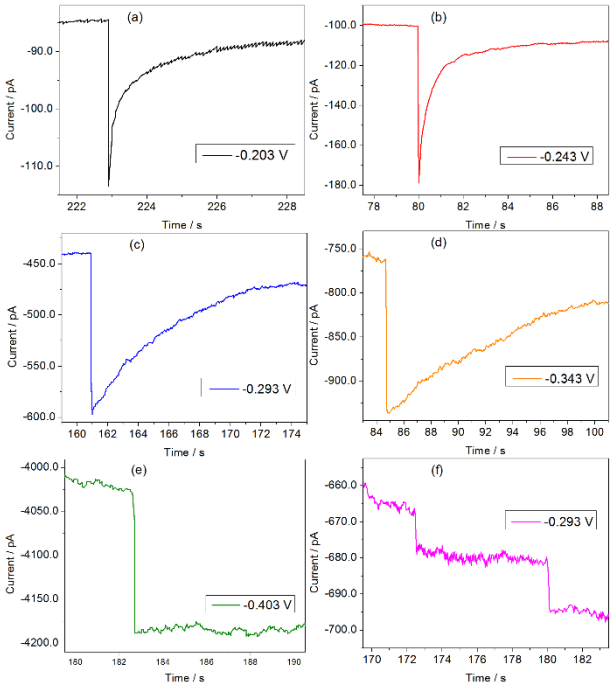

Figure S9. Zoom-in graphs of current transients from Pt NPs collision events towards HER at different potentials (*vs*. SHE): (a−e) in helium-saturated 1.0 mM $HClO_4$ solution, (f) in hydrogen-saturated 1.0 mM $HClO_4$ solution.

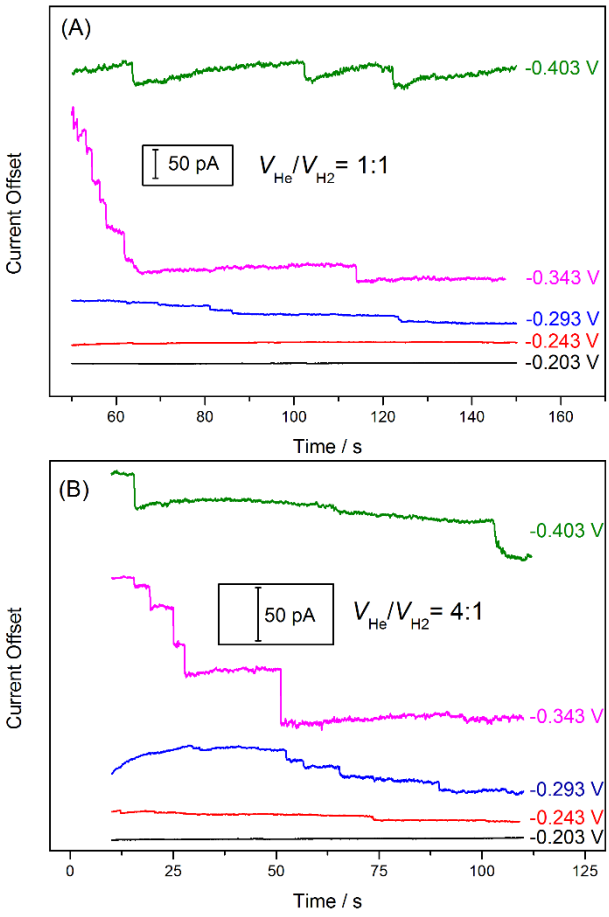

Figure S10. Chronoamperometry of Pt NP collision events towards HER at different potentials (*vs.* SHE) under the hydrogen partial pressure of (A) 0.5 and (B) 0.2.

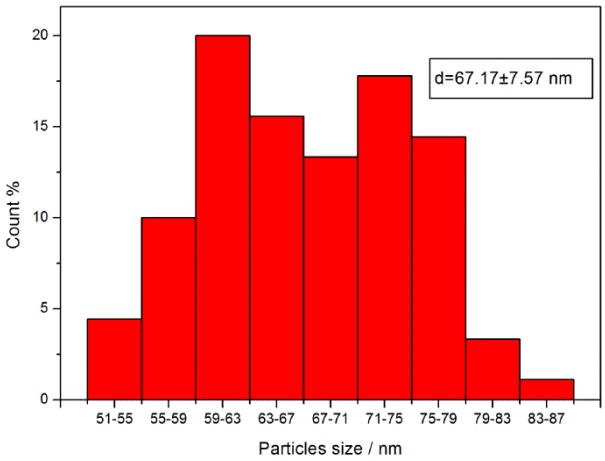

Figure S11. Size distribution of the Pt NPs calculated from current transient values of 90 collision events recorded at the potentials from −0.293 to −0.403 V in He-saturated 1.0 mM $HClO_4$ (refer to Figure 1A in the main text).

The steady-state current in Figure 1A in the main text can be used to calculate the NP's size distribution by Equation S13,[6, 16]

$$I = 4\pi(\ln 2)nFD_{H^+}C_{H^+}r_p \quad \text{(S13)}$$

where I is the diffusion-controlled current generated at a single NP in contact with an infinitely-large planar surface, D_{H^+} is the diffusion coefficient of proton (9.3×10^{-5} cm^2 s^{-1}),[17] C_{H^+} is the concentration of proton (0.63 mM H^+ for 0.58 pM 70-nm citrate-Pt NPs in 1.0 mM $HClO_4$), n is 1 for electron transfer in HER, F and r_p have been defined before. The average diameter of the NPs is calculated to be *ca*. 67 nm (see Figure S11), which coincides well with the SEM result (average diameter: ~71 nm, see Figure S1 and Table S1).

The Au UME was assumed to be inert to the HER in the COMSOL simulations. The experimental CVs in Figures S8 and S12 (*vide infra*) show that the proton reduction current is negligible and as low as −0.808 nA at −0.403 V, which is the lowest potential utilized for experimental electrochemical collision studies. To quantitatively verify that this approach is justified, we have accordingly done some additional simulations. If we assume that the current density distribution follows the distribution established for the limiting current (as given for example in *Electroanalysis* 1993, 5, 627-639), we can calculate the steady-state concentrations considering the experimental current at −0.403 V. The results show that the proton concentration decreases by 2.7 % from the bulk concentration, indicating that the effect of the proton reduction on the Au UME is indeed negligible. And the current on the NP should correspondingly decrease by ~3%, leading to a slight underestimation of the NP size.

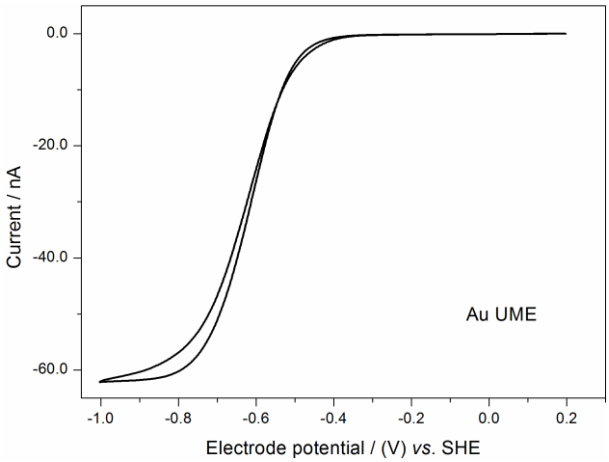

Figure S12. CV of HER on Au UME (25 μm in diameter) in He-saturated 1.0 mM $HClO_4$ solution at a scan rate of 50 mV s^{-1} (*vs.* SHE).

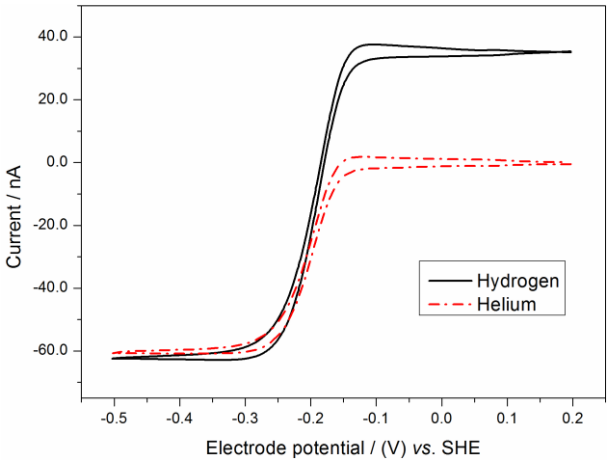

Figure S13. CVs of Pt UMEs (25 µm in diameter) in He-saturated (red dash-dotted curve) and H_2-saturated (100 ml min^{-1}, black curve) 1.0 mM $HClO_4$ solution recorded at 50 mV s^{-1} (*vs.* SHE).

COMSOL Multiphysics simulations

The equilibrium concentrations of both hydrogen and proton were obtained by the finite element method using COMSOL Multiphysics, as seen in Table S5. Note that the Pt catalyst passivation was not considered in the model. The comparison to COMSOL simulations under He in Figure 2A in the main text actually compares experimental current spikes (except the current steps experimentally obtained at −0.403 V) *vs*. computed current steps.

The details of the simulations are as follows.

i) The HER follows the Volmer-Tafel mechanism ($H^+ + e^- + Pt \leftrightarrow$ H-Pt and 2H-Pt $\leftrightarrow H_2 + 2Pt$);

ii) Steady state is applied in the simulations to obtain the surface (*i.e.* NP/electrolyte interface) concentration;

iii) The Pt NP radius is 35 nm, the proton concertation is 0.63 mM, and other parameters are used from the publications of Compton *et al*.;[3, 18]

iv) The initial hydrogen concentration is estimated from CV with the Pt UME by using the limiting current of hydrogen oxidation reaction (Figure S2, Table S2), which agrees well with the calculation from the Henry's law (Equation S11). The four initial bulk hydrogen concentrations given in Table S5 correspond to the solutions respectively saturated with pure He, 4:1 He/H_2, 1:1 He/H_2, and pure H_2.

Table S5. The simulated steady-state current and equilibrium concentrations at different applied potentials (*vs.* SHE) in solutions with different initial hydrogen concentrations.

0 mM H_2				**0.158 mM H_2**			
E, V	*I*, pA	[H^+], mM	[H_2], mM	*E*, V	*I*, pA	[H^+], mM	[H_2], mM
–0.0991	–0.02	0.63	6×10^{-5}	–0.0991	7.7	0.65	0.13
–0.203	–29	0.54	0.09	−0.203	–25	0.55	0.23
–0.243	–88	0.36	0.27	−0.243	–87	0.36	0.42
–0.293	–146	0.16	0.44	−0.293	–146	0.17	0.60
–0.343	–173	0.07	0.52	−0.343	–173	0.07	0.68
–0.403	–185	0.02	0.56	−0.403	–185	0.02	0.72
0.398 mM H_2				**0.79 mM H_2**			
E, V	*I*, pA	[H^+], mM	[H_2], mM	*E*, V	*I*, pA	[H^+], mM	[H_2], mM
–0.0991	19	0.69	0.34	–0.0991	38	0.74	0.67
–0.203	–20	0.57	0.46	−0.203	–12	0.59	0.83
–0.243	–86	0.36	0.66	−0.243	–83	0.37	1.04
–0.293	–145	0.17	0.84	−0.293	–145	0.17	1.23
–0.343	–173	0.07	0.92	−0.343	–173	0.07	1.31
–0.403	–185	0.02	0.96	−0.403	–185	0.02	1.35

It is seen in the investigated potential range, the equilibrium concentration of hydrogen is always far from being saturation (0.79 mM) in the two former cases. And at lower potentials (*e.g.* −0.203 V), the steady-state current of the HER decreases as the initial concentration of hydrogen increases.

Finally, it should be pointed out that in the simulations, hydrogen leaves the NP surface by diffusion, rather than by nucleation of hydrogen bubbles. We exclude the bubble formation based on the following observations. Figure S13 reveals that the limiting current curve of the HER is smooth during the potential scan even in H_2-saturated solution, which intuitively suggests that the

steady-state diffusion of proton is not blocked and the bubble formation is insignificant on a micron-scale Pt disk electrode. One may raise the concern about the possible bubble formation on a nano-scale Pt particle. We further performed the experiment with 4:1 He/H_2 mixture, in which hydrogen is unsaturated in the investigated potential range (*vide supra*). In comparison, in H_2-saturated solution, the equilibrium concentration of hydrogen at −0.403 V reaches high up to 1.35 mM, which is seriously super-saturated at the interface. It is interesting to note that the current magnitudes are the same in the two cases (see Figure 2 in the main text). As such, the formation of bubbles is excluded from consideration as the bubbles will block the diffusion of protons.

References

[1] a) F. R. F. Fan, J. Fernandez, B. Liu, J. Mauzeroll, C. G. Zoski, in *Handbook of Electrochemistry* (Ed.: C. G. Zoski), Elsevier, Amsterdam, **2007**, pp. 189-199; b) Z. Liang, H. S. Ahn, A. J. Bard, *J. Am. Chem. Soc.* **2017**, *139*, 4854-4858.

[2] A. J. Bard, L. R. Faulkner, *Electrochemical Methods*, 2nd ed., John Wiley & Sons, New York, **2001**.

[3] X. Jiao, C. Batchelor-McAuley, E. Kätelhön, J. Ellison, K. Tschulik, R. G. Compton, *J. Phys. Chem. C* **2015**, *119*, 9402-9410.

[4] a) A. Bard, A. Boika, S. Kwon, J. Park, S. Thorgaard, in *Nanoelectrochemistry*, CRC Press, **2015**, pp. 241-292; b) A. J. Bard, H. Zhou, S. J. Kwon, *Isr. J. Chem.* **2010**, *50*, 267-276; c) W. Cheng, R. G. Compton, *TrAC Trends Anal. Chem.* **2014**, *58*, 79-89.

[5] X. Xiao, A. J. Bard, *J. Am. Chem. Soc.* **2007**, *129*, 9610-9612.

[6] X. Xiao, F. R. F. Fan, J. Zhou, A. J. Bard, *J. Am. Chem. Soc.* **2008**, *130*, 16669-16677.

[7] R. Dasari, B. Walther, D. A. Robinson, K. J. Stevenson, *Langmuir* **2013**, *29*, 15100-15106.

[8] H. Deng, J. E. Dick, S. Kummer, U. Kragl, S. H. Strauss, A. J. Bard, *Anal. Chem.* **2016**, *88*, 7754-7761.

[9] J. Kestin, M. Sokolov, W. A. Wakeham, *J. Phys. Chem. Ref. Data* **1978**, *7*, 941-948.

[10] V. Brasiliense, A. N. Patel, A. Martinez-Marrades, J. Shi, Y. Chen, C. Combellas, G. Tessier, F. Kanoufi, *J. Am. Chem. Soc.* **2016**, *138*, 3478-3483.

[11] P. Peljo, J. A. Manzanares, H. H. Girault, *Chem. Sci.* **2017**, *8*, 4795-4803.

[12] a) S. Eloul, R. G. Compton, *J. Phys. Chem. Lett.* **2016**, *7*, 4317-4321; b) E. Katelhon, R. G. Compton, *Chem. Sci.* **2014**, *5*, 4592-4598; c) S. V. Sokolov, S. Eloul, E. Katelhon, C. Batchelor-McAuley, R. G. Compton, *Phys. Chem. Chem. Phys.* **2017**, *19*, 28-43.

[13] a) S. Levine, *Proc. R. Soc. Lond. A* **1939**, *170*, 145-164; b) S. Levine, *Proc. R. Soc. Lond. A* **1939**, *170*, 165-182.

[14] P. W. Atkins, *Physical Chemistry, 4th ed.*, Oxford University Press, Oxford, **1990**.

[15] L. Luo, H. S. White, *Langmuir* **2013**, *29*, 11169-11175.

[16] P. A. Bobbert, M. M. Wind, J. Vlieger, *Physica A* **1987**, *141*, 58-72.

[17] S. H. Lee, J. C. Rasaiah, *J. Chem. Phys.* **2011**, *135*, 1245051-12450510.

[18] X. Jiao, C. Lin, N. P. Young, C. Batchelor-McAuley, R. G. Compton, *J. Phys. Chem. C* **2016**, *120*, 13148-13158.